

# Yielding transition of amorphous solids in the presence of aspherical impurities

Anoop Mutneja,<sup>1,\*</sup> Bhanu Prasad Bhowmik,<sup>2,†</sup> and Smarajit Karmakar<sup>1,‡</sup>

<sup>1</sup>*Tata Institute of Fundamental Research, 36/P, Gopanpally Village,  
Serilingampally Mandal, Ranga Reddy District, Hyderabad, Telangana 500107, India*

<sup>2</sup>*School of Engineering, The University of Edinburgh,  
King's Buildings, Edinburgh EH9 3FG, United Kingdom*

Understanding the mechanical properties of amorphous solids is a crucial area of research due to the fascinating phenomena they exhibit under external deformations and their importance in industrial applications. Although these solids have higher yield strength compared to crystalline solids of similar composition, they often fail catastrophically through shear band formation. Tuning their mechanical behavior is vital for material design. Engineers have long been seeking ways to improve the ability of amorphous solids to withstand external deformations, with micro-alloying being a popular method. By adding small amounts of different materials to pure samples, micro-alloying can enhance yield strain, although the microscopic mechanisms behind this process remain poorly understood. We conducted a study with extensive molecular dynamics simulations on model amorphous solids to investigate the effect of asphericity of the impurity particles on their yielding behaviour. Our results indicate that aspherical impurities free to rotate can significantly increase the yield threshold. Conversely, when impurities are unable to rotate, they can lead to the formation of extremely brittle, ultrastable-like systems. The rotational degrees of freedom are controlled by changing the aspect ratio of the impurity, and they play a crucial role in influencing shear band formation. Additionally, we found that including larger impurities enhances the structural stability of the parent glass matrix.

## I. INTRODUCTION

The investigation of mechanical failure in amorphous solids holds paramount significance owing to its extensive application in both industrial and everyday life contexts. While the mechanical behavior of crystalline solids subjected to external deformation is comprehensively elucidated in terms of defects associated with their structure, such defects cannot be precisely delineated in amorphous solids due to the absence of long-range structural order. As a result, despite rigorous research efforts [1–3], the mechanical response of amorphous solids continues to elude a comprehensive understanding.

Under external deformation, amorphous solids exhibit a combination of elastic and plastic responses [4–7]. As strain increases, stress undergoes non-linear growth, attributed to stress drops (plastic events) resulting from the irreversible rearrangement of constituent particles. In the initial stages of straining a freshly prepared sample, plastic events are small and spatially localised [8] with a quadrupolar structure in displacement field, well-known in the literature from the exact results in Eshelby inclusion problem [9]. However, with increasing strain, their size and frequency amplify. Consequently, beyond a certain threshold of strain, stress ceases to increase, marking the onset of mechanical failure or fluidization of the solids. This phenomenon is recognized as the yield transition of materials. Despite decades of research, a clear understanding of how an amorphous

solid yield remains elusive, with one set of studies suggesting it as a non-equilibrium phase transition [10–14] while the other studies argue this as a purely a dynamic crossover [15]. Depending on the nature of the failure, one can distinguish between “ductile” and “brittle” yielding. In the former case, material flow is a gradual process facilitated by the proliferation of plasticity in the system, such as the flow of foam or various pastes. In the latter case, the system experiences catastrophic failure through the sudden formation of a system-spanning shear band instability, as observed in the breaking of metallic glass. However, the same material may exhibit either form of yielding, contingent upon the sample’s stability [11, 16, 17] or size [18–21]. Creating a highly stable sample and optimizing its mechanical strength are popular research topics in the field.

The stability of the computer glass formers can be controlled by changing the cooling rates during the preparation [22]; a lower cooling rate will give a more stable sample. However, even the lowest accessible cooling rate results in a poorly annealed state, making it difficult to study realistic systems. However, highly stable glassy configurations can be prepared using the swap Monte-Carlo method in computer simulations (known as ultrastable glasses) [23, 24] in polydisperse system [11] and with the use of cyclic deformation [25, 26]. While swap Monte-Carlo is not readily applicable to experiments, cyclic shear protocols might not guarantee kinetic stability and generate very well-annealed glasses [26–28]. Recently, ultrastable glass was obtained using random bonding [29], which can be considered a potential technique to generate realistic stable glasses in patchy colloids

\* [anoop.mutneja2011@gmail.com](mailto:anoop.mutneja2011@gmail.com)

† [bhowmikbhanuprasad592@gmail.com](mailto:bhowmikbhanuprasad592@gmail.com)

‡ [smarajit@tifrh.res.in](mailto:smarajit@tifrh.res.in)

besides vapor deposition techniques [30].

Another important aspect of these studies is to have control on the alteration of the mechanical strength of the materials. For decades, engineers have been working on ways to improve the ability of amorphous solids to sustain external loading. One popular method is micro-alloying, which involves adding small amounts of different materials to the pure sample [31, 32]. While there are many examples of how micro-alloying [33, 34] can improve the yield strain, the microscopic mechanism behind it has yet to be fully understood. Recent studies have focused on the role of impurities in the mechanical response of amorphous solids, particularly through particle pinning [35, 36]. This technique has been shown to prevent plastic events and delay the yielding transition; moreover, random pinning leads to a transition from heterogeneous to homogeneous yielding.

Using computer simulation of a binary glass-forming system, we investigate the effect of impurities on the yielding transition of amorphous solids in the athermal quasi-static scenario in the context of micro-alloying. We used both spherical and aspherical impurities and analyzed the stability of the obtained sample along with the microscopics behind the attained mechanical strength. In the case of spherical impurities, we add a third type of particle into the glass matrix, which has a larger diameter than the constituent particles. In the case of aspherical impurities, we add rod-shaped particles into the glass matrix. In recent studies, rod-shape particles are proven to be useful in studying growing length scales of glassy systems [37–39] and jamming transition in granular systems [40]. The advantage of using rod-shaped impurities over spherical impurities is that they introduce rotational degrees of freedom (DoF) in the system, which provides extra pathways for stress relaxation under mechanical loading.

We find that adding large spherical impurities improves the prepared glassy state’s structural order, reducing the plasticity at smaller strains, increasing the yield strain, and leading to more brittle type yielding. Aspherical dimers, having comparatively the same size as large particles, on the other hand, exhibit a similar but enhanced response; the system can sustain a much larger load than spherical impurities. We prove this to be linked with the extra rDoF. We also study the effect of increasing rod length on the yield point and found that such long rods (with large rotational inertia) change the yielding transition to be highly brittle type, similar to ultra-stable glasses. We connect this observation with the decreasing rotational degrees of freedom of aspherical impurities with their increasing length. Our study thus points towards the enhancement of strain-bearing capacity with the presence of rDoF, while frozen rDof will lead to ultra-stable-like behaviour as also observed in a recent work [29].

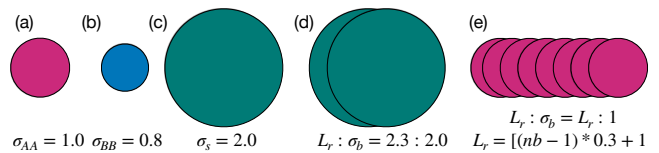


FIG. 1. **Components of the system** : (a, b) Particle type ‘A’ and ‘B’ of the parent KA system. (c) The spherical impurity with twice the diameter of the particle ‘A’. It has a variable number fraction of  $c_s$  in the system. (d) A dimer made with larger particles and having a slight asphericity. We have varied their number fraction ( $c_r$ ) in the system (e) Rods with larger aspect ratio, made by attaching A-type particles. We studied the systems with different aspect ratio rods, with a fixed number fraction of  $c_r = 0.1$ .

## II. MODEL SYSTEMS & SIMULATION DETAILS

We conduct simulations of a binary Kob-Anderson mixture of Lennard-Jones particles in both two and three dimensions. The model details are as follows:

**3d model:** The 3D Kob-Anderson model (referred to as 3D) [41] represents a binary mixture comprising A- and B-type Lennard-Jones particles, with a concentration ratio of 80 : 20. This generic model resembles molecular glass-forming liquid,  $Ni_{80}P_{20}$ . The following potential governs the interaction between particles:

$$V_{\alpha\beta}(\mathbf{r}) = 4\epsilon_{\alpha\beta} \left[ \left( \frac{\sigma_{\alpha\beta}}{r} \right)^{12} - \left( \frac{\sigma_{\alpha\beta}}{r} \right)^6 \right] \quad (1)$$

where  $\alpha$  and  $\beta$  vary in A, B and the interaction strengths and radii are  $\epsilon_{AA} = 1.0$ ,  $\epsilon_{AB} = 1.5$ ,  $\epsilon_{BB} = 0.5$ ;  $\sigma_{AA} = 1.0$ ,  $\sigma_{BB} = 0.88$  and  $\sigma_{AB} = 0.8$ . The interaction is truncated at  $r = 2.5\sigma_{\alpha\beta}$  and is smoothed by adding up to  $2^{nd}$  order terms.

**2d model:** 2d modified Kob-Anderson model (mentioned as 2d) [42] is the glass forming model in 2 dimensions with properties like 3dKA. It is a 65:35 binary mixture of the same A and B particles of the 3dKA model interacting with the same potential and parameters.

**Rods and spherical dopants:** In the glass formers mentioned above, we added  $c_r$  ( $c_s$ ) concentration of rods (spherical particles) in the parent system of  $N = (1 - c_r)N_T$  particles; we used a system with  $N_T = 100000$  total particles. Each rod is formed by glueing  $nb$  spheres at a fixed distance of  $d = 0.3\sigma_{AA}$ . In this study, to achieve the soft pinning effect, the rods are made up of two beads each with diameter of  $\sigma_b = 2.0$ , while  $\sigma_{b,\alpha} = 0.5(\sigma_b + \sigma_\alpha)$ , same is true for the spherical dopants; while they have same mass and interacts via same potential as parent spheres with  $\epsilon_{b,\alpha} = 1$  and  $\epsilon_{b,b} = \frac{1}{2}$  for both the models.  $\epsilon_{b,b} = \frac{1}{2}$  is chosen to avoid the nematic ordering. The aspect ratio of such a dimer will be  $L_r : \sigma_b = 2.3 : 2$ . We have also studied the mechanical response with thin rod inclusions with  $\sigma_b = 1.0$ . The aspect ratio of such a dopant will be  $L_r : \sigma_b = (nb - 1) * 0.3 + 1 : 1$ .

**Sample preparation:** The moderately-annealed state of a glassy system with  $c_r$  ( $c_s$ ), the concentration of rods (spherical dopants) is prepared by firstly equilibrating the system at high temperature ( $T = 0.5$ ). It is then slowly cooled to temperature  $T = 5 \times 10^{-4}$ , with a cooling rate of  $dT/dt = 1 \times 10^{-4}$ . This annealed state is minimized via conjugate-gradient to reach the inherent state (IS). This inherent state is then used as a starting point for all shear procedures.

**Shear protocol:** This work focuses only on the athermal quasi-static ( $T \rightarrow 0$  and  $\dot{\gamma} \rightarrow 0$ ) deformation. We start with an inherent state and deform it by increasing the strain by  $\delta\gamma = 5 \times 10^{-5}$  in every step. Each deformation step contains two parts; the first step is called affine transformation, in which particle positions are modified in the following way:  $x_i = x_i + \delta\gamma y_i$ ,  $y_i = y_i$ ,  $z_i = z_i$ . Here the strain is applied in the  $x$  direction. The second step involves minimizations of energy in which particles are brought back to mechanical equilibrium. We use the conjugate gradient method for energy minimization.

**Structural order parameter:** The structural order parameter utilized in this study aims to characterize the deviation of local structure from perfect steric packing, as outlined in Ref. [43]. The specific order parameter, denoted as  $\Theta_o$  for a tagged particle  $o$ , is determined through a series of steps detailed next. Firstly, the neighbours of  $o$  are identified using radical Voronoi tessellation, then sets of four particles, comprising the tagged particle  $o$  and three of its neighbours, are identified to form tetrahedra. For each bond within the tetrahedron, the imperfection is calculated as  $\sum_{\langle ab \rangle} |r_{ab} - \sigma_{ab}|$ , where  $\langle ab \rangle$  ranges over the six edges of the tetrahedron, and  $\sigma_{ab} = (\sigma_a + \sigma_b) \times 0.5$  represents the favoured distance. Normalization is applied, and the imperfections are averaged over all tetrahedra. The order parameter for a particle is then given by the expression:

$$\Theta_o = \frac{1}{N_0^{tetra}} \sum_{oijk} \frac{\sum_{\langle ab \rangle} |r_{ab} - \sigma_{ab}|}{\sum_{\langle ab \rangle} \sigma_{ab}} \quad (2)$$

where  $\langle oijk \rangle$  runs over all tetrahedron sets. The system's structural order parameter is computed by averaging over all particles. A higher value of  $\Theta_o$  indicates a more disordered local surrounding; thus, the  $\Theta$  map serves as a valuable tool for identifying regions with shear bands, as elaborated in the results section.

For systems with dopants, to directly compare structural order parameters,  $\Theta_o$  is averaged only over the parent liquid particles. Additionally, for  $\Theta_o$  calculation, only tetrahedra containing parent particles are considered, while Voronoi tessellation is performed on all particles, including the beads of each rod.

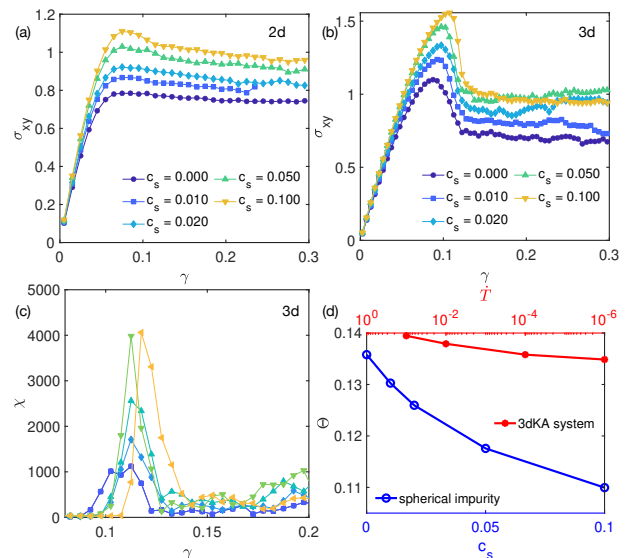


**FIG. 2. Mechanical properties with spherical inclusions:** (a, b) Stress-strain curves for the 2dmKA and 3dKA systems with different  $c_s$ ; the systematic shift in the yield point to higher strain values with increasing the concentration of ternary particles can be seen. Panel (c) shows the susceptibility plot (Eq.3) for the 3d system with changing  $c_s$ . The shifted peaks and increased sharpness conclude the increase in yield point and emerging brittle-like behaviour. (d) The structural order parameter is shown for the  $\gamma = 0$  state of the system with different concentrations of inclusions (blue), along with its comparison with the states generated using different cooling rates (red). It shows the increased structural stability of the glass matrix with increasing  $c_s$  and not so much with decreasing cooling rate.

### III. RESULTS

#### A. Increasing mechanical strength with spherical impurities

First, we investigate the bulk mechanical behavior of the system by incorporating spherical impurities (Fig1(c)) in the spirit of micro-alloying. Generally, impurities have two adjustable parameters: their size and the strength of their interaction with the system's constituent particles. While the latter has been studied in the past [44], we focus on the effect of size by introducing larger impurities with a diameter of  $\sigma_s = 2\sigma_{AA}$  for a range of concentration  $c_s$  from 0 – 10% into the system of total particle (constitutive particles and impurities)  $N_T = 100000$ . We conduct a strain-controlled experiment on the 2-dimensional modified KA and 3-dimensional KA glass-forming systems, with the stress acting as the observable. Fig. 2(a) and 2(b) illustrate the stress-strain curves for both models, respectively. The results clearly indicate an increase in both the yield strain and the shear modulus ( $\mu$ ) with an increasing concentration of impurities in systems of both dimensions. The enhancement of mechanical strength is also accompanied

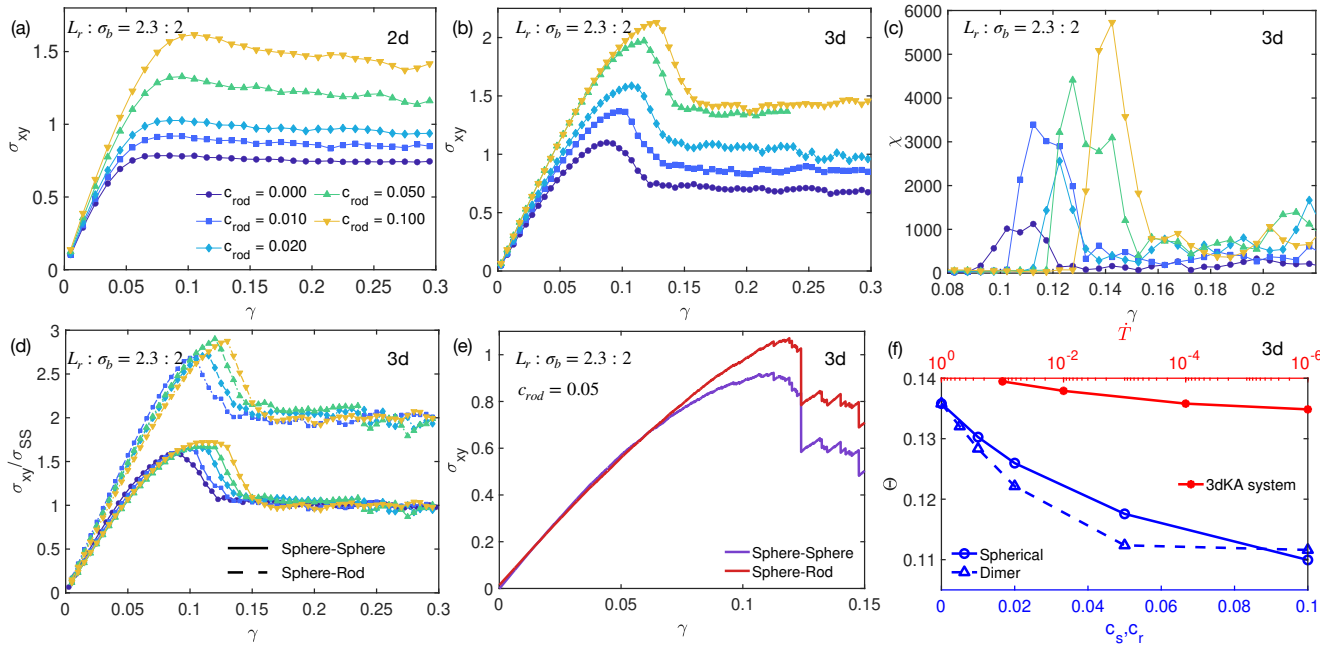


FIG. 3. **Mechanical properties with aspherical inclusions:** (a, b) Stress-strain curves for 2dmKA and 3dKA system with different  $c_r$ ; the systematic shift in the yield point to higher strain values, almost 100% improvement compare to the ternary system is seen; Panel (c) is the susceptibility plots for the three dimension system. The increase in peak height and the shift in peak to larger strain value with increasing  $c_r$  supports the conclusion of increased yield strain. Panel (d) shows the stress contributions from sphere-sphere and sphere-rod bonds, normalized by the steady-state values. The rods-sphere pairs are making the system hold stress to larger strain values, where the sphere-sphere stress has already started to fall. Panel (e) shows the single ensemble version of the same for  $c_r = 0.05$ . Panel (f) compares the structural order parameter of the system with spherical inclusions (circles) and aspherical inclusions (triangles). The similar trend and change in the magnitude suggest the similarity in the  $\gamma = 0$  structure. However, the huge change in yielding strain points to the importance of rDoFs.

by a prominent stress peak, especially for the 3D KA model, along with an increase in steady-state stress values (flow stress). On top of that, the yielding seems to become more brittle in nature. Generally, the nature of the yielding transition can be characterized by computing the susceptibility,

$$\chi(\gamma) = N_T (\langle \sigma_{xy}^2 \rangle - \langle \sigma_{xy} \rangle^2). \quad (3)$$

$\chi(\gamma)$  has a maximum at the yield point but exhibits a sharp peak for brittle failure. A sharper peak with a larger magnitude indicates a more brittle character of the yield process. In Fig.2(c), we show how  $\chi$  becomes sharper, and the peak height of  $\chi$  increases with increasing  $c_s$ , signifying the emerging brittle character in our system. The peak also shifts to larger strain values, manifesting the higher yield strain in the system. The mechanical response of the systems with impurities indicates the enhanced structural stability of the samples. The most common method to characterize the stability of the amorphous solid is the energy per particle averaged over all the all particles of the system. However, in our system, due to the addition of foreign particles, the energy scale with different concentrations might not remain comparable. Thus, to delve deeper into this observation, we rely on the structural order parameter [43], denoted by  $\Theta$  (Eq.2), which depends purely on the local struc-

ture rather than the interaction. The lower value of the structural order parameter stands for the better stability of the system. We compute  $\Theta$  of the unstrained configurations (freshly prepared samples) for all  $c_s$ , shown in Fig.2(d). We find that a lowering of  $\Theta$  with increasing  $c_s$  indicates enhanced structural stability, aligning with the observed brittle behavior. For comparison, we include the influence of the cooling rate on  $\Theta$  in the same plot (red points), revealing its minimal impact even across three decades of slowing down compared to the effect of large spherical impurities. We note that in our study, the diameter of the impurity is limited to  $1.8 - 2.0\sigma_{AA}$ . While smaller impurities have a very mild effect, the larger impurity system cannot be equilibrated within the available simulation time scale due to their slow dynamics.

## B. Increasing mechanical strength using aspherical impurities

Although the results with spherical impurities are encouraging, we must admit that the improvement is minimal ( $\gamma_Y(c_s = 0) = 0.09$  to  $\gamma_Y(c_s = 0.1) = 0.107$  for the 3D KA system). Interestingly, studies in [29, 35, 45] highlight the significant impact of eliminating degrees of freedom on the mechanical properties of amorphous



solids. In contrast, we focus on the alternation in the mechanical properties of amorphous solids brought about by the introduction of rotational degrees of freedom (rDoFs) through rod-like aspherical impurities, as discussed in the following sections.

### 1. Effect of impurity concentration

To begin with, we examine the response of less aspherical rod-shape impurities (Fig. 1(d)) for various impurity concentrations  $c_d$ . The volume of these impurities is chosen to be similar to that of spherical impurities, aiming to impart a comparable influence on the system as the larger spherical impurities, as demonstrated by the structural order parameter in Fig. 3(f). However, compared to spherical impurities, they possess additional rotational degrees of freedom. These impurities are created by attaching two spheres (beads) with a diameter of  $\sigma_b = 2.0\sigma_{AA}$ , with a 77.7% overlap, resulting in a length of  $L_d = 2.3\sigma_{AA}$  and an aspect ratio of  $L_d : \sigma_b = 2.3 : 2$ . Given that these impurities consist solely of two beads, we designate them as dimers to differentiate them from another category of impurities that comprise more than two beads with the same amount of overlap described later in the paper. Various parameter of the dimer impurity system is denoted by the subscript ‘ $d$ ’ if not mentioned otherwise. Fig. 3(a, b) shows the stress-strain curves for the studied model systems. Notably, we observe a significant increase in yield strain for both two and three dimensions, accompanied by a substantial increase in the shear modulus. For instance, in the 3D KA model, the yield strain changes by around 40% from  $\gamma_Y = 0.09$  for the pure systems to  $\gamma_Y = 0.127$  for  $c_d = 10\%$ , compared to around 18% for the system with spherical impurities. Additionally, the stress overshoots become more pronounced with higher dimer concentrations. This systematic increase in the yield point with larger  $c_d$  suggests that small dimer impurities render the system more stable and capable of withstanding greater loads than the pure system. This observation is further supported by the  $\chi(\gamma)$  plots shown in Fig. 3(c); shift in the peak position to a larger strain indicates an increase in  $\gamma_Y$  with increasing  $c_d$ , while the increased peak height indicates improved stability rather than increased brittleness, as the width of the  $\chi$  vs.  $\gamma$  curve remains very similar with increasing  $c_d$ . We note that the rod impurities with aspect ratio  $L_r : \sigma_b = 1.3 : 1$  give qualitatively similar results, although the change in different mechanical properties is less prominent. We do not study the dimer with a larger diameter as the equilibration of the system stands as a problem.

To microscopically understand the role of rod impurities in enhancing the system’s stability and delaying the yielding transition, we analyzed stress contributions from rod-sphere and sphere-sphere interactions at a microscopic level, as shown in Fig. 3, panel (d). The data for all studied concentrations reveal that the stress con-

tribution from sphere-sphere interaction begins to saturate at smaller strains than the system’s macroscopic yield strain, whereas the stress contribution from the rod-sphere interaction keeps increasing until the yield strain and then starts decreasing sharply. This indicates that the regions with rods are more structurally stable and deform plastically at higher strain values than those without rods. This also suggests that the onset of yielding is mainly controlled by the rod-sphere interaction, depicting a clear picture of delayed yielding with increasing  $c_d$ .

Fig. 3 (f) illustrates the enhanced structural stability of the parent glass matrix in terms of  $\Theta$  as the  $C_d$  increases. The figure also shows the variation of  $\Theta$  with concentration of spherical impurities and with different cooling rates for comparison. It’s important to note that the structural stability introduced by both spherical and aspherical particles is similar in magnitude. This can be attributed to the fact that the volume of a rod is comparable to that of a spherical impurity. However, the substantial shift in the yield point for the aspherical case indicates a significant influence of rotational degrees of freedom on the yielding transition. By providing additional pathways for dissipating internal stresses, these degrees of freedom allow the system to dissipate extra stresses. In the subsequent section, we explore the system containing rod-shaped impurities of varying lengths to test this assertion further, where such impurities with longer lengths inherently exhibit reduced rotational freedom.

### 2. Effect of the length of rod dopant

We now add longer rod-shaped impurities (more aspherical compared to dimer) in the amorphous matrix (see Fig. 1(e)). These impurities have more than two beads and, for clarity, are identified as rods. The subscript  $r$ , if not mentioned otherwise, indicates various parameters associated with the rod impurity system. The diameter of each bead in the rod is kept to be  $\sigma_r = \sigma_{AA}$ . The reason to reduce the bead diameter from  $2\sigma_{AA}$  to  $\sigma_{AA}$  is that long rods with large diameters exhibit very slow dynamics and can not be equilibrated within the available simulation time scale. Even with a smaller bead, the maximum rod length we can simulate is  $L_r = 2.5\sigma_{AA}$ . Fig. 4(a) shows the averaged stress-strain curve for a 3dKA system with rod concentration  $c_r = 0.1$  of different  $L_r$ . One can clearly see that for samples with the rod,  $L_r = 1.3$  has large  $\gamma_Y$  compared to the pure samples due to the presence of rotational degrees of freedom, but the yield point is shifting back to lower values with increasing  $L_r$ , akin to the fact of reduced rotational relaxation of the longer rods. The degree of rotational relaxation can be characterized by the rotational relaxation function defined as  $S_r = \langle \frac{1}{N_r} \sum_{i=1}^{N_r} \hat{s}_i(\gamma) \cdot \hat{s}_i(0) \rangle$  shown in Fig. 4(b). Here  $\hat{s}_i$  is the orientation vector of the rod. A faster decay of  $S_r$  suggests a better independent

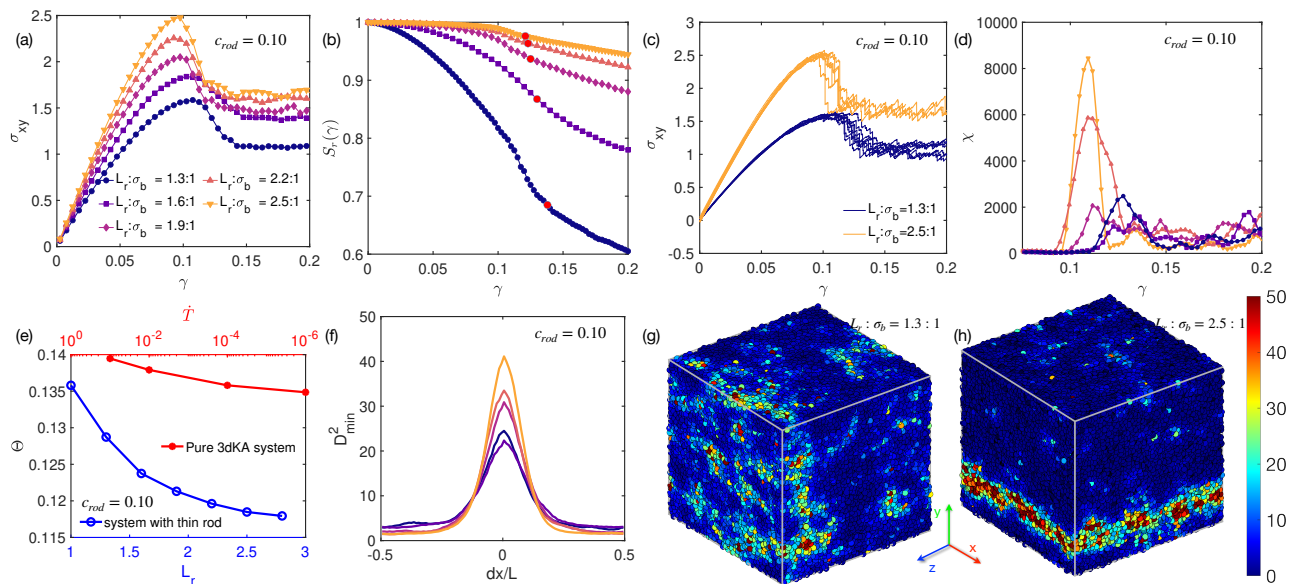


**FIG. 4. Mechanical properties with longer rod inclusions:** (a, b) The stress-strain curves for 2dmKA and 3dKA systems with different lengths of rods (Fig.1(e)). Firstly, the yield point shifts back with increasing rod length because of losing rDoFs, which is shown in panel (b). Panel (b) shows the rotational decorrelation function for rods of different lengths with mechanical loading; the red points indicate the equal net  $D_{min}^2$  [46]. Secondly, Panel (a) suggests the increased brittle behaviour with increasing rod length. It is further advocated in (c-h). Panel (c) shows brittle (not so brittle) behaviour in sample-to-sample stress-strain plots for systems with rods of length  $L_r = 2.5$  ( $L_r = 1.3$ ). The sharpness and increased peak height of  $\chi$  in (d) also convey the emerging mechanical ultra-stability of the sample. (e) The structural order parameter decreases with increasing rod length in the system, implying increased structural stability. Panel (f) shows the non-affine displacement  $D_{min}^2$ , averaged in strips perpendicular to the shear band (at  $dx = 0$ ). All these curves have the same area under the curve to ensure equal plasticity. The large displacement away from the shear band in systems with smaller rods and large peak value for longer rods again advocate the emerging brittle behaviour. It is also clear from the  $D_{min}^2$  maps (g, h) obtained at equal net displacements for systems with rods of lengths  $L_r = 1.3$  and  $L_r = 2.5$ , respectively.

mobility of the rod's orientation. We see  $S_r$  decreases with  $\gamma$  for all  $L_r$  due to the non-affine motion originating from the plastic events. However, systems with different  $L_r$  do not suffer from the same amount of plasticity at the same  $\gamma$ . So we choose  $S_r$  at different  $\gamma$  shown by the red points on the data where all the systems have the same amount of net non-affine displacement (in terms of total  $D_{min}^2$ ). The higher values of  $S_r$  at the point of the same plasticity with increasing  $L_r$  advocate the reduced rotational motion of larger rods.

Another clear facet emerging from the average stress-strain curves is the increased brittle behaviour with increasing rod length. It is also worth pointing out that the system with longer rods is dynamically slow; thus, the same preparation protocol would generate poorly annealed states, which should smoothen the stress-strain curve; implying that the observed brittleness is even stronger than what we obtain in this study because of the simulation difficulty. In Fig. 4(c), the individual stress-strain curves of two different  $L_r$  are compared. For  $L_r = 1.3$ , the stress-strain curves exhibit several stress drops near the yielding transition. On the other hand, for  $L_r = 2.5$ , the individual stress-strain curves are more abrupt, and larger stress drops occur during plastic events, indicating the emergence of shear band instability

in the system. Fig. 4(d) displays the large values of the  $\chi(\gamma)$  peak, which becomes narrower with increasing  $L_r$ , indicating an emerging mechanically ultra-stable phase for longer rods. In panel (e), the variation of  $\Theta$  is presented as a function of rod length for samples prepared using the same cooling rate.  $\Theta$  decreases with increasing  $L_r$ , suggesting better stability of the samples. Although yield strain should increase with higher stability, such a trend is not observed. Thus, one can easily conclude that with increasing  $L_r$ , the lack of rDoF would push  $\gamma_Y$  to lower  $\gamma$ , whereas the higher stability of the system should do the opposite, but the system yields at smaller  $\gamma_Y$  as the effect of rDoFs dominates over the effect of stability of the systems.

As a direct indicator of increased brittle behavior, Fig. 4(f) presents the non-affine displacement,  $D_{min}^2$  [46], averaged across slices perpendicular to the shear band, and plotted against the distance from the center of the shear band for systems with rods of varying lengths. All the curves have similar areas under the curve to ensure the same amount of plasticity. The plots show that the non-affine displacement magnitude away from the shear band decreases with increasing rod length, indicating less spatially scattered plastic events. Furthermore, the peaked displacement for larger rods shows the formation

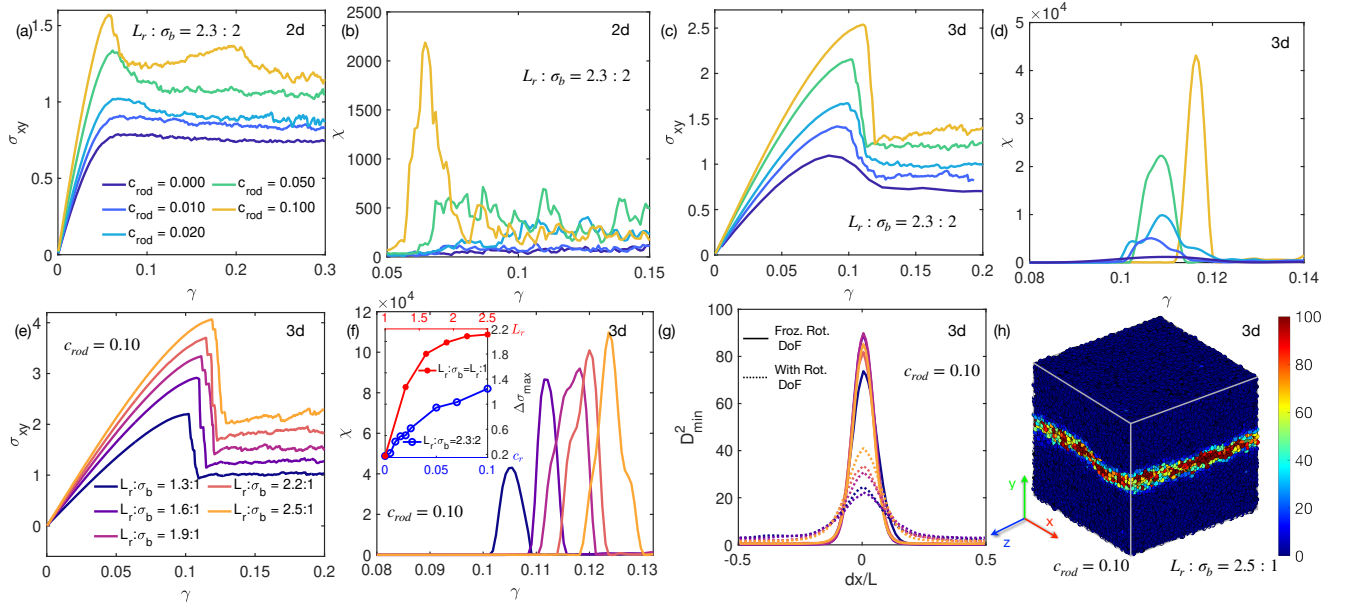


FIG. 5. **Mechanical aspect of frozen rotational DoFs:** (a, c) The averaged stress-strain curves for 2dmKA and 3dKA systems with rotationally frozen dimer (Fig.1(d)) inclusions. The yield strain does not change much, and the system becomes extremely brittle, as seen from the respective susceptibility plots in panels (b, d). Note for the 3dKA model, the stress-strain curves become nearly discontinuous at the yielding transition for the larger concentration of dimers. The effect is even enhanced for the system with more aspherical rods (panel (e, f)). Inset of (f) contains the averaged maximum stress drop ( $\Delta\sigma_{max}$ ) that happened in the whole strain window. It is an order parameter for brittle behaviour [11], and its systematic increased magnitude with increasing rod concentration and rod length proves that the frozen rDoF leads to a highly brittle breakdown. Panel (g, h) shows the  $D_{min}^2$  plots indicating the sharpness of the obtained shear band (see text for detailed discussion).

of shear band. The same can be seen from  $D_{min}^2$  map of the system with  $L_r = 1.3$  in Fig. 4(g), and with  $L_r = 2.5$  in Fig. 4(h). For a direct comparison, these two maps have an equal net  $D_{min}^2$ , and it is evident that the system with shorter rods has multiple plastic events that are spatially spread out, while the longer rods have a localized shear band. Thus, the emerging ultra-stability originates from the lack of rotational freedom, as we will see in the next section.

### C. Ultra-stability with Frozen Rotational DoFs

#### 1. Mechanical aspect

Our results presented in Fig. 4 demonstrate that with increasing rod length, the rotational diffusivity decreases significantly, indicating the possibility of complete arrest of rotation after a certain rod length. However, the effect of such long rods cannot be observed due to simulation limitations. Nonetheless, in a realistic system, it is possible to freeze rDoFs at a suitable temperature and rod length [37, 47]. To overcome this numerical difficulty and mimic the effect of very long rods that have vanishing rotational diffusivity, we manually freeze the rDoFs by prohibiting the rod-shape impurities from rotating during the stress release via minimization process (non-affine motion), although rotation is allowed during

the affine transformation.

The same samples for different concentrations of dimer impurities and for different rod lengths of rod impurities used in the previous analysis are taken and subjected to straining with frozen rDoFs. Fig. 5(a) and Fig. 5(c) show the stress-strain curves for the systems in two and three dimensions, with frozen rotational DoFs. Firstly, the drastic increase in the yield strain shown in Fig. 3 has disappeared, re-confirming the vital role of the rotational degrees. Although  $\gamma_Y$  increases slightly with increasing  $c_d$  due to the higher stability of the system captured by  $\theta$  in Fig. 3, panel (f). Secondly, in Fig. 5(b), we show the susceptibility,  $\chi$  for the 2dmKA model, the peak height increase with a significant decrease in the width of the  $\chi - \gamma$  curves points to the increasing brittle-like failure. The trend in the 3dKA model is even dramatic as shown in Fig. 5(d), in which one sees the stress-strain curve to become nearly discontinuous at the transition point and the corresponding susceptibility  $\chi$  attaining a very large peak value with a smaller spread in the loading axis. In Fig. 5(e), the stress-strain curve is shown for various  $L_r$  for  $c_r = 0.1$ . For all values of  $L_r$  the failure is brittle, but longer rod impurities increase the shear modulus due to the higher stability of the samples (see Fig. 4, panel (e)), and cause the failure to become more brittle as implied from the peak height of  $\chi$  shown in panel (f). Another important measure for quantifying brittle behavior is the maximum stress drop, denoted as  $\Delta\sigma_{max}$  [11]. This

parameter is computed as the maximum stress drop in a unit step that occurs within the entire strain window. The average value of  $\Delta\sigma_{max}$ , denoted as  $\langle \Delta\sigma_{max} \rangle$ , is zero for macroscopic ductile systems and non-zero for brittle systems. The inset of Fig. 5 (f) displays the values  $\Delta\sigma_{max}$ , where one can observe a systematic increase with both increasing rod length (red line), and concentration of dimers (blue line), confirming the more brittle behavior.

Figure 5(g) tries to bring out the change in the yielding process with and without rDoFs. It shows the spatial variation of the non-affine displacement,  $D_{min}^2$ , similar to Fig. 4(f) w.r.t to the distance from the center of the shear band for both cases. The extremely small displacement outside the shear band for the frozen rDoFs scenario, along with increased displacement in the shear band region, demonstrates the highly brittle nature of the failure. This is also supported by the  $D_{min}^2$  map in panel (h) of Fig. 5.

## 2. Kinetic aspect

After demonstrating their enhanced mechanical stability, we now focus on the kinetic stability of systems with frozen rDoFs. To assess the kinetic stability of a solid, we observe the potential energy per particle ( $e$ ) while subjecting it to heating-cooling cycles. An ultra-stable state would be characterized by a deep potential energy minimum that can not be reached through normal cooling, therefore resulting in hysteresis in the potential energy plot. To test this, we melted the rotationally frozen system of 10% dimers with larger beads by heating it to temperature  $T = 1.8$  with  $\dot{T} = 10^{-4}$  and then cooled it down to the same temperature using the same  $\dot{T}$ . The cooling or heating rate is kept the same as the rate with which the sample was prepared. Note that while preparing the sample, the rDoFs were not frozen but during the heating/cooling cycles, they are kept frozen as we are interested in the gained kinetic stability due to the lack of rDoFs. As shown in Fig. 6(a), hysteresis is observed, validating the classical ultra-stable characteristics. Upon heating, the system remained in its glassy state until  $T = 1.12$ , while on cooling, it reached its glassy state at  $T = 1.0$ , resulting in a glass with a higher potential energy per particle. However, the second heat cycle did not exhibit hysteresis. Furthermore, the absence of hysteresis in the dashed lines of Fig. 6(a), which depict the same procedure with rotationally free rods, confirms the effectiveness of fRoDs in creating ultra-stable glasses. The specific heat ( $C_V = de/dT$ ) plots in Fig. 6(b) also support this conclusion.

## IV. DISCUSSION

Our results demonstrate that incorporating impurities of larger diameter into a glassy system can significantly

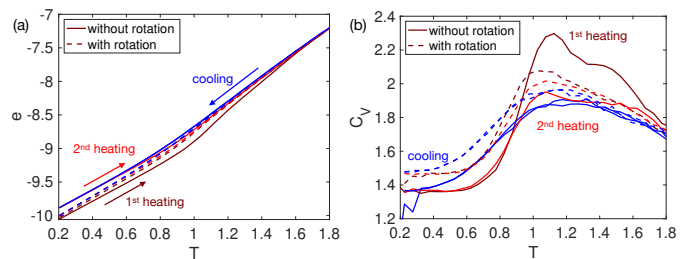


FIG. 6. **Kinetic aspect of frozen rotational DoFs:** (a) The potential energy per particle  $e$  is plotted for a system with 10% dimers subjected to heating-cooling cycles at the rate of  $dT/dt = 10^{-4}$  (same as the rate with which the sample was prepared). The solid lines are for a system with frozen rotational DoFs; the observed hysteresis during the first cycle indicates the ultra-stable character. The second heating cycle does not show any hysteresis. The dashed lines are for the system evolved with rotational DoFs, and the absence of hysteresis is seen as expected. (b) The specific heat  $C_V = de/dT$  is calculated from data in (a) by numerical differentiation and conveys the same

increase its ability to withstand external loads beyond its usual limit, along with increased shear modulus and yield stress. Furthermore, rod-shaped asymmetric inclusions, which have both translational and rotational degrees of freedom, are much better for micro-alloying as they can significantly increase the yield strain, shear modulus, as well as yield stress at even small concentrations. Conversely, inclusions with frozen or constrained rotational degrees of freedom, which can be achieved by increasing the length of the rod impurities while keeping the diameter the same, exhibit comparatively mild enhancement of the yield strain but fail in a more brittle-like catastrophic yielding transition, suggesting the ultra-stable nature of the system. Recently, in Ref.[29], the bulk-ultra stable glass phase was claimed to be formed by randomly bonding the nearest neighbors of an otherwise poorly annealed glassy state. Such bonded molecules would also be rotationally stuck because of the packing. Thus our results offer an alternate explanation of the results reported in [29].

The observation of the long/rotationally stuck dopant making the system behave in a highly brittle way can be hypothesized as an effect of the larger length scale in the system. The ultra-stable states are sampled from extremely low temperatures, implying a sizable structural length scale, while the states sampled from high temperatures would have a structural length scale of a few particle diameters. By inserting a rod of length  $L_r$ , a static correlation of the same length is induced. Thus the observed similarity between systems doped with larger rod-like dopant and ultra-stable glasses may be simply due to the increased static correlation length. Although we do not have direct proof of this argument, it seems more likely to be the scenario, and further work is needed to understand the microscopic reason for the strong similarity between ultra-stable glasses and micro-alloyed glasses



with long rod-like impurities. Finally, it is worth noting that incorporating aspherical impurities into realistic amorphous solids can be achieved quite easily. This enables us to tune the amorphous matrix's mechanical properties by varying the impurities' length. While a spherically symmetric impurity lacks rotational Degrees of Freedom (rDoFs), the addition of slightly asymmetric impurities with the same or larger radius as the constituent particles results in a significant increase in both the yield strain and stress of the material due to the addition of these rDoFs. Conversely, the incorporation of highly aspherical rod-like impurities transforms the system into one that more closely resembles an ultra-stable configuration. Thus, our findings open a more controlled

and systematic method of micro-alloying.

## V. ACKNOWLEDGMENT

SK acknowledges funding by intramural funds at TIFR Hyderabad from the Department of Atomic Energy (DAE) under Project Identification No. RTI 4007. Core Research Grant CRG/2019/005373 and Swarna Jayanti Fellowship SB/SFJ/2019-20/05 from Science and Engineering Research Board (SERB) are acknowledged for generous funding. Most of the computations are done using the HPC clusters bought using CRG/2019/005373 grant and Swarna Jayanti Fellowship, grants DST/SJF/PSA01/2018-19, and SB/SFJ/2019-20/05 of SK.

- 
- [1] J.-L. Barrat and A. Lemaitre, Heterogeneities in amorphous systems under shear, in *Dynamical Heterogeneities in Glasses, Colloids, and Granular Media* (Oxford University Press, 2011) pp. 264–297.
- [2] A. Nicolas, E. E. Ferrero, K. Martens, and J.-L. Barrat, Deformation and flow of amorphous solids: Insights from elastoplastic models, *Rev. Mod. Phys.* **90**, 045006 (2018).
- [3] D. Bonn, M. M. Denn, L. Berthier, T. Divoux, and S. Manneville, Yield stress materials in soft condensed matter, *Rev. Mod. Phys.* **89**, 035005 (2017).
- [4] H. G. E. Hentschel, S. Karmakar, E. Lerner, and I. Procaccia, Do athermal amorphous solids exist?, *Phys. Rev. E* **83**, 061101 (2011).
- [5] C. E. Maloney and A. Lemaître, Amorphous systems in athermal, quasistatic shear, *Phys. Rev. E* **74**, 016118 (2006).
- [6] C. Maloney and A. Lemaître, Subextensive scaling in the athermal, quasistatic limit of amorphous matter in plastic shear flow, *Phys. Rev. Lett.* **93**, 016001 (2004).
- [7] S. Karmakar, E. Lerner, I. Procaccia, and J. Zylberg, Statistical physics of elastoplastic steady states in amorphous solids: Finite temperatures and strain rates, *Phys. Rev. E* **82**, 031301 (2010).
- [8] S. Karmakar, E. Lerner, and I. Procaccia, Statistical physics of the yielding transition in amorphous solids, *Phys. Rev. E* **82**, 055103 (2010).
- [9] J. D. Eshelby and R. E. Peierls, The determination of the elastic field of an ellipsoidal inclusion, and related problems, *Proceedings of the Royal Society of London. Series A. Mathematical and Physical Sciences* **241**, 376 (1957).
- [10] S. K. Nandi, G. Biroli, and G. Tarjus, Spinodals with disorder: From avalanches in random magnets to glassy dynamics, *Phys. Rev. Lett.* **116**, 145701 (2016).
- [11] M. Ozawa, L. Berthier, G. Biroli, A. Rosso, and G. Tarjus, Random critical point separates brittle and ductile yielding transitions in amorphous materials, *Proceedings of the National Academy of Sciences* **115**, 6656 (2018).
- [12] M. Popović, T. W. J. de Geus, and M. Wyart, Elastoplastic description of sudden failure in athermal amorphous materials during quasistatic loading, *Phys. Rev. E* **98**, 040901 (2018).
- [13] P. K. Jaiswal, I. Procaccia, C. Rainone, and M. Singh, Mechanical yield in amorphous solids: A first-order phase transition, *Physical Review Letters* **116**, 10.1103/physrevlett.116.085501 (2016).
- [14] G. Parisi, I. Procaccia, C. Rainone, and M. Singh, Shear bands as manifestation of a criticality in yielding amorphous solids, *Proceedings of the National Academy of Sciences* **114**, 5577 (2017).
- [15] P. Nath, S. Ganguly, J. Horbach, P. Sollich, S. Karmakar, and S. Sengupta, On the existence of thermodynamically stable rigid solids, *Proceedings of the National Academy of Sciences* **115**, E4322 (2018).
- [16] M. Singh, M. Ozawa, and L. Berthier, Brittle yielding of amorphous solids at finite shear rates, *Physical Review Materials* **4**, 10.1103/physrevmaterials.4.025603 (2020).
- [17] S. Rossi, G. Biroli, M. Ozawa, G. Tarjus, and F. Zampori, Finite-disorder critical point in the yielding transition of elastoplastic models, *Phys. Rev. Lett.* **129**, 228002 (2022).
- [18] H. J. Barlow, J. O. Cochran, and S. M. Fielding, Ductile and brittle yielding in thermal and athermal amorphous materials, *Phys. Rev. Lett.* **125**, 168003 (2020).
- [19] J. Pollard and S. M. Fielding, Yielding, shear banding, and brittle failure of amorphous materials, *Phys. Rev. Res.* **4**, 043037 (2022).
- [20] D. Richard, C. Rainone, and E. Lerner, Finite-size study of the athermal quasistatic yielding transition in structural glasses, *The Journal of Chemical Physics* **155**, 10.1063/5.0053303 (2021), 056101.
- [21] A. L. Greer, Metallic glasses, *Science* **267**, 1947 (1995).
- [22] A. J., E. Bouchbinder, and I. Procaccia, Cooling-rate dependence of the shear modulus of amorphous solids, *Phys. Rev. E* **87**, 042310 (2013).
- [23] T. S. Grigera and G. Parisi, Fast monte carlo algorithm for supercooled soft spheres, *Phys. Rev. E* **63**, 045102 (2001).
- [24] R. Gutiérrez, S. Karmakar, Y. G. Pollack, and I. Procaccia, The static lengthscale characterizing the glass transition at lower temperatures, *Europhysics Letters* **111**, 56009 (2015).
- [25] B. P. Bhowmik, V. Ilyin, and I. Procaccia, Thermodynamic equivalence of cyclic shear and deep cooling in

- glass formers, *Phys. Rev. E* **102**, 010603 (2020).
- [26] H. Bhaumik, G. Foffi, and S. Sastry, The role of annealing in determining the yielding behavior of glasses under cyclic shear deformation, *Proceedings of the National Academy of Sciences* **118**, 10.1073/pnas.2100227118 (2021).
- [27] V. V. Krishnan, K. Ramola, and S. Karmakar, Annealing effects of multidirectional oscillatory shear in model glass formers, *Phys. Rev. Appl.* **19**, 024004 (2023).
- [28] W.-T. Yeh, M. Ozawa, K. Miyazaki, T. Kawasaki, and L. Berthier, Glass stability changes the nature of yielding under oscillatory shear, *Phys. Rev. Lett.* **124**, 225502 (2020).
- [29] M. Ozawa, Y. Iwashita, W. Kob, and F. Zamponi, Creating bulk ultrastable glasses by random particle bonding, *Nature Communications* **14**, 10.1038/s41467-023-35812-w (2023).
- [30] M. D. Ediger, Perspective: Highly stable vapor-deposited glasses, *The Journal of Chemical Physics* **147**, 10.1063/1.5006265 (2017), 210901.
- [31] G. R. Garrett, M. D. Demetriou, J. Chen, and W. L. Johnson, Effect of microalloying on the toughness of metallic glasses, *Applied Physics Letters* **101**, 241913 (2012).
- [32] S. González, Role of minor additions on metallic glasses and composites, *Journal of Materials Research* **31**, 76 (2015).
- [33] J. S. Harmon, M. D. Demetriou, W. L. Johnson, and K. Samwer, Anelastic to plastic transition in metallic glass-forming liquids, *Phys. Rev. Lett.* **99**, 135502 (2007).
- [34] G. R. Garrett, M. D. Demetriou, J. Chen, and W. L. Johnson, Effect of microalloying on the toughness of metallic glasses, *Applied Physics Letters* **101**, 241913 (2012).
- [35] B. P. Bhowmik, P. Chaudhuri, and S. Karmakar, Effect of pinning on the yielding transition of amorphous solids, *Physical Review Letters* **123**, 10.1103/physrevlett.123.185501 (2019).
- [36] B. P. Bhowmik, S. Karmakar, I. Procaccia, and C. Rainone, Particle pinning suppresses spinodal criticality in the shear-banding instability, *Phys. Rev. E* **100**, 052110 (2019).
- [37] A. Mutneja and S. Karmakar, Probing dynamic heterogeneity and amorphous order using rotational dynamics of rodlike particles in supercooled liquids, *Phys. Rev. Applied* **16**, 034022 (2021).
- [38] A. Mutneja and S. Karmakar, Translational dynamics of a rod-like probe in supercooled liquids: an experimentally realizable method to study stokes–einstein breakdown, dynamic heterogeneity, and amorphous order, *Soft Matter* **17**, 5738 (2021).
- [39] I. Tah, A. Mutneja, and S. Karmakar, Understanding Slow and Heterogeneous Dynamics in Model Supercooled Glass-Forming Liquids, *ACS Omega* **6**, 7229 (2021).
- [40] A. V. Kyrylyuk, M. Anne van de Haar, L. Rossi, A. Wouterse, and A. P. Philipse, Isochoric ideality in jammed random packings of non-spherical granular matter, *Soft Matter* **7**, 1671 (2011).
- [41] W. Kob and H. C. Andersen, Testing mode-coupling theory for a supercooled binary lennard-jones mixture i: The van hove correlation function, *Phys. Rev. E* **51**, 4626 (1995).
- [42] R. Brüning, D. A. St-Onge, S. Patterson, and W. Kob, Glass transitions in one-, two-, three-, and four-dimensional binary lennard-jones systems, *Journal of Physics: Condensed Matter* **21**, 035117 (2008).
- [43] H. Tong and H. Tanaka, Structural order as a genuine control parameter of dynamics in simple glass formers, *Nature Communications* **10**, 10.1038/s41467-019-13606-3 (2019).
- [44] O. Gendelman, A. Joy, P. Mishra, I. Procaccia, and K. Samwer, On the effect of microalloying on the mechanical properties of metallic glasses, *Acta Materialia* **63**, 209–215 (2014).
- [45] Y. Liu, H. Liu, and H. Peng, Pinning effect on the correlations of nonaffine displacement in metallic glasses, *Journal of Non-Crystalline Solids* **601**, 122052 (2023).
- [46] M. L. Falk and J. S. Langer, Dynamics of viscoplastic deformation in amorphous solids, *Physical Review E* **57**, 7192 (1998).
- [47] F. R. Blackburn, C.-Y. Wang, and M. D. Ediger, Translational and rotational motion of probes in supercooled 1, 3, 5-tris(naphthyl)benzene, *The Journal of Physical Chemistry* **100**, 18249 (1996).